



HAL
open science

Oxide spin-orbitronics: New routes towards low-power electrical control of magnetization in oxide heterostructures

Diogo Castro Vaz, Agnès Barthélémy, Manuel Bibes

► **To cite this version:**

Diogo Castro Vaz, Agnès Barthélémy, Manuel Bibes. Oxide spin-orbitronics: New routes towards low-power electrical control of magnetization in oxide heterostructures. *Japanese Journal of Applied Physics*, 2018, 57 (9), pp.0902A4. 10.7567/JJAP.57.0902A4 . hal-02331561

HAL Id: hal-02331561

<https://hal.science/hal-02331561>

Submitted on 27 Oct 2019

HAL is a multi-disciplinary open access archive for the deposit and dissemination of scientific research documents, whether they are published or not. The documents may come from teaching and research institutions in France or abroad, or from public or private research centers.

L'archive ouverte pluridisciplinaire **HAL**, est destinée au dépôt et à la diffusion de documents scientifiques de niveau recherche, publiés ou non, émanant des établissements d'enseignement et de recherche français ou étrangers, des laboratoires publics ou privés.

Oxide spin-orbitronics: New routes towards low-power electrical control of magnetization in oxide heterostructures

D.C. Vaz¹, A. Barthélémy^{1*}, and M. Bibes^{1*}

¹*Unité Mixte de Physique CNRS/Thales, Univ. Paris-Sud, Université Paris Saclay, 91767 Palaiseau, France*

*E-mail: agnes.barthelemy@cnrs-thales.fr, manuel.bibes@cnrs-thales.fr

The transition metal oxide family harbors various types of materials of interest for spintronics: half-metallic manganites are highly efficient spin injectors and detectors, yielding record values of tunnel magnetoresistance; multiferroic materials, and in particular BiFeO₃, allow the electrical control of magnetization and spin excitations at room temperature; combined with ferromagnets, piezoelectric perovskites enable a controlled tuning of magnetic anisotropy, domain dynamics and even magnetic order. In this review, we argue that a new opportunity is emerging for oxides in spintronics with the rise of spin-orbit-driven phenomena such as the direct and inverse spin Hall and Rashba-Edelstein effects. After surveying the few results reported on inverse spin Hall measurements in oxide materials, we describe in depth the physics of SrTiO₃-based interfaces and their usage for both spin-to-charge and charge-to-spin conversion. Finally, we give perspectives for a more thorough exploration of spin Hall effects in oxides and enhanced conversion ratios in both three- and two-dimensional structures.

1. Introduction: Electrical control of magnetization

Spintronics utilizes both the charge and spin degrees of freedom of electrons to store, transmit and process information¹⁾. Historically, spin-based information has been recorded by the magnetization direction in a ferromagnetic metal – typically a transition metal alloy based on Co, Fe and/or Ni – and manipulated by the application of a magnetic field generated by current lines. Although this approach led to a first generation of non-volatile magnetic random-access memories (MRAM), commercialized in 2006, their design and very large power consumption prevented reaching higher storage densities. A first technological breakthrough towards denser memories came with the discovery of spin-transfer torque, a mechanism by which a spin-polarized current running through a ferromagnet is able to switch its magnetization²⁾. This led to simpler and more compact designs as well as a significant reduction in write energies, remaining however one to two orders of magnitude above desirable values.

Interestingly, the first experimental demonstration of spin-transfer torque magnetization switching was reported in 1999³⁾, almost concomitant with the rediscovery of magnetoelectric multiferroics⁴⁾, an important family of materials that attracted a huge attention in the following decades^{5,6)}. Multiferroics are appealing for spintronics because they possess at least two ferroic (or antiferroic) order parameters (often being ferroelectric and magnetic) that can be coupled, which provides a route to control magnetism electrically⁷⁾. Importantly, multiferroics are insulators, meaning that they are not controlled through the application of an electrical current – as with spin-transfer torque – but by an electric field, allowing much lower power consumption together with non-volatility (in contrast with approaches based on dielectrics such as MgO⁸⁾).

The route from the concept of magnetoelectric switching using multiferroic materials to its practical realization has been long and tortuous⁹⁻¹²⁾. Reasons include the virtual inexistence of ferroelectrics with a large magnetization, imposing the need to combine multiferroics with ferromagnets, the limited number of room-temperature multiferroics and the modest amplitude of the magnetoelectric coupling. However, recent results^{13,14)} have aroused the interest of major electronics companies^{15,16)}, boosting the use of multiferroics in next-generation spin-based transistors that require ultralow power consumption.

While oxide materials have only played a small part in the development of spin-transfer torque, they have been at the heart of the research on multiferroics, with materials such as BiFeO₃ – a room-temperature ferroelectric with non-collinear antiferromagnetic order –

on the spotlight¹⁷⁾. Additionally, materials such as SrTiO₃ are starting to be used to convert charge currents into spin currents, opening new doors for spintronic devices that operate without external magnetic fields. In this review, we will discuss the potential of oxide materials for the low-power electrical control of magnetism through spin-orbit-based mechanisms. With conventional materials such as heavy metals, this approach already allows a decrease of power required to switch magnetization in current-based schemes and aims to rival the performance of magnetoelectric switching, providing enhanced endurance and exciting prospects for spin-current detection. As we explain hereinafter, oxides may have an unanticipated but essential role to play in this new arena.

2. Direct and inverse spin Hall and Rashba-Edelstein effects

A new paradigm for magnetization manipulation aims at harnessing pure spin currents from charge currents, in materials or interfaces with large spin-orbit interactions. This concept is at the heart of spin-orbitronics, where the interplay between charge and spin currents is exploited via spin-to-momentum coupling, enabled by the spin-orbit coupling (SOC). Two important physical effects that allow the creation of pure spin currents from charge currents (and vice versa) are the spin Hall effect (SHE^{18,19)} and inverse spin Hall effect (ISHE^{20,21)}), both observed in bulk materials with SOC (see Figure 1a). Their origin is attributed to either extrinsic effects, such as impurity scattering, or intrinsic effects of the SOC on the band structure. Moreover, the conversion factor between charge and spin currents is set by the spin Hall angle (θ_H), i.e., the ratio between a 3D spin current (j_s) and a 3D charge current (j_c). An advantage of the SHE and ISHE over electrical spin injection is that they realize spin-to-charge interconversion without using a ferromagnetic conductor and thus circumvent drawbacks like the intrinsic limitation of the transferred angular momentum per unit charge observed in conventional spin torque experiments. Indeed, spin currents generated by the SHE in non-magnetic heavy metals have been shown to efficiently generate spin-orbit transfer torques that are able to control the magnetization of a FM material^{22,23)}, move magnetic domain walls²⁴⁾, generate magnetic oscillations²⁵⁾ or amplify spin waves^{26,27)} in heavy metal/ferromagnet bilayers; all of this with a reduced power consumption.

Recently, the realization of efficient spin-to-charge interconversion in two-dimensional electron gases (2DEG), at surfaces of topological insulators or in semiconductor quantum wells (via SOC) has been widely recognized and has attracted much attention. At these interfaces (surfaces), due to their two-dimensional nature, the combination of the spatial

symmetry breaking, that results in a built-in electric potential along the direction normal to the interface (or surface) \vec{z} , and SO interaction is at the essence of the so-called Rashba effect²⁸). The corresponding Rashba Hamiltonian can be expressed as $H_R = \alpha_R(\vec{k} \times \vec{\sigma}) \cdot \vec{z}$, where $\vec{\sigma}$ is the vector of the Pauli spin matrices, \vec{k} the momentum and α_R the Rashba coefficient, proportional to the electric field strength and the SO interaction. In a Rashba system the momentum and spin degrees of freedom are locked (Figure 1b) and the spin degeneracy of the 2D band structure is lifted (see light dashed lines in Figure 1c corresponding to the steady state). When a charge current flows along -x, it will induce an equal shift by Δk_x of both inequivalent Fermi contours (Figure 1c, black lines), thus yielding a spin accumulation with polarization along y; an effect called the Rashba-Edelstein effect (REE). This spin accumulation can diffuse in an adjacent conducting material through the interface and generate a pure 3D spin current without net charge current. Conversely, when a spin accumulation is induced at the interface, by injection of a spin current along \vec{z} , the two inequivalent Fermi contours are shifted in equal magnitude but opposite directions (see dark lines in Figure 1d), yielding a net charge current along -x; an effect called the Inverse Rashba-Edelstein Effect (IREE). The efficiency of this effect can be estimated with its figure of merit, λ_{IREE} , given by the ratio between the 2D charge current generated, j_c^{2D} , and the 3D spin current injected, j_s^{3D} . Note that since one current is 2D and the other 3D, λ_{IREE} has the dimension of a length and is usually expressed in nm. In the simplest case of circular contours, λ_{IREE} is also proportional to the Rashba coefficient α_R and the relaxation time τ , so that $\lambda_{IREE} = \frac{\alpha_R \tau}{\hbar}$. A way to optimize the spin-to-charge conversion is thus to find interfaces housing large electric fields (together with large SOC) or even to use external gate voltage to tune the Rashba SOC (as we demonstrate further ahead). For the REE, the charge-to-spin current conversion efficient is given by q_{REE} , which represents the ratio between the 3D spin current generated and the 2D charge current injected.

In principle, spin-to-charge interconversion through the REE and IREE does not satisfy the Onsager reciprocity due to the inequivalence of the considered spin currents. The efficiency of the IREE, given by $\lambda_{IREE} = \frac{j_c^{2D}}{j_s^{3D}}$, is calculated with the spin current injected into the Rashba interface (by spin pumping for example), whereas for the REE the conversion efficiency (previously introduced in spin torque ferromagnetic resonance (ST-FMR) experiments^{29,30}) is similarly given as $q_{REE} = \frac{j_s^{3D}}{j_c^{2D}}$. It must be noted that the

definition of j_s^{3D} is not the same in these two experiments. When performing spin pumping, the broadening of the FMR line gives the final spin current j_s^{3D} injected into the 2DEG after crossing the interface, so that λ_{IREE} does not depend on the transmission by the interface but only on the intrinsic properties of the Rashba system³¹⁾. In contrast, in ST-FMR experiments, j_s^{3D} is the spin current absorbed by the magnetic material, so that q_{REE} depends on both the intrinsic properties of the Rashba system and the interface transmission³²⁾.

Several experiments performed at interfaces with large Rashba SOC between two metals^{33–36)}, two-dimensional materials^{35,37–39)} and topological surfaces states^{40–45)} have also recently been considered for the realization of the REE and IREE effects, opening a route to an efficient control of magnetization at lower energy consumption^{42,46)}. From here on, we address the potential of transition metal oxides for efficient spin-to-charge interconversion.

3. Inverse and direct spin Hall with oxide materials

The investigation of the direct and inverse spin Hall effects in oxide conductors is in its infancy and systematic studies as a function of structural parameters or across materials families are still lacking. The first experimental measurement of an inverse spin Hall effect in an oxide was in indium-tin oxide (ITO) through spin-pumping experiments from a La-doped yttrium iron garnet (La-YIG) thin film⁴⁷⁾. No details on the structural quality of the ITO films were provided, but it can be assumed that they were polycrystalline films. Indeed, one of the advantages of ITO is that highly conductive films can be grown on top of it, without a strong dependence on their crystalline quality or epitaxial nature. A few months later, similar experiments were reported with ITO combined with a NiFe film and a small spin Hall angle $\theta_{\text{SHE}}=0.0065\pm 0.001$ was determined⁴⁸⁾.

While ITO contains In and Sn, two 4d elements, oxides based on heavier atoms with strong atomic spin-orbit coupling are potentially more interesting candidates to realize a strong spin-to-charge interconversion via spin Hall effects. Indeed, working with amorphous and polycrystalline IrO₂ thin films, Fujiwara et al. were able to measure a spin Hall angle of $\theta_{\text{SHE}}=0.065$ and 0.04 respectively through nonlocal ISHE experiments in lateral spin-valves with NiFe electrodes⁴⁹⁾. Combined with its high resistivity, this large SHE angle makes IrO₂ a promising material for the detection of spin currents at room temperature.

Finally, to this date spin Hall angle measurements have been done for only one perovskite

material, SrRuO₃, combined into epitaxial heterostructures with La_{0.7}Sr_{0.3}MnO₃ (LSMO) used as a spin injector. Below T_C=160 K, SrRuO₃ is a ferromagnet, and ISHE has been demonstrated both in its paramagnetic phase and down to 50 K below T_C. The maximum response was $\theta_{\text{SHE}}=-0.027\pm 0.018$ at 190 K.

While the oxide perovskite family is mostly known for its members possessing ferroic properties (ferroelectrics, ferromagnetic metals and multiferroics⁵⁰), it also comprises a number of non-magnetic conductors based on 3d, 4d and 5d elements, as illustrated in Table 1. With LSMO now established as an efficient spin injector (with Gilbert damping coefficients as low as $5\cdot 10^{-4}$ (Ref. ⁵¹)) and thus better than most ferromagnetic metals), such conductive oxides could be advantageously integrated into high-quality epitaxial spintronics architectures to assess their spin Hall response. In particular, it would be interesting to explore trends across the 4d and 5d row as well as to probe the role of crystal orientation and of possible interface dipoles.

4. Inverse and direct Rashba-Edelstein effect in SrTiO₃-based heterostructures

In the search for alternative systems to explore 2D Rashba physics, oxide interfaces emerge as prominent candidates, for their exotic and unusual electronic properties. The acclaimed LaAlO₃/SrTiO₃ (LAO/STO) system serves as a great example of an all-oxide system that exhibits fascinating properties such as interfacial conductivity with high mobilities⁵²), superconductivity⁵³) and traces of magnetism^{54–56}). Additionally, Caviglia et al.⁵⁷) showed that the quasi two-dimensional electron gas formed at the interface also shows strong gate-tunable Rashba SOC, ideal for further exploration of spin-to-charge interconversion.

Several groups have since then confirmed this effect through magnetotransport^{58–61}) and theory^{62–64}), using both the LAO/STO interface as well as other STO-based systems⁶⁵). Importantly, one unique feature of these systems is that the Rashba SO coupling is extremely dependent on the position of the Fermi level, hinting for the potential use of external gate voltages to tune the effect.

In bulk SrTiO₃, the cubic crystal field lifts the degeneracy of the 3d orbitals, so that the energy of the t_{2g} triplet is lowered with respect to the e_g doublet. The t_{2g} triplet, forming the conduction band, is composed of three degenerate ellipsoidal Fermi surfaces centered in the Γ point and aligned along the main lattice directions. At the LAO/STO interface, when

a 2DEG is formed, the degeneracy is lifted due to the perpendicular confining electric field that breaks inversion symmetry. In this scenario, a light d_{xy} band is split towards lower energy [76] with respect to the other two heavier d_{xz} and d_{yz} bands. At low carrier densities, hence low Fermi level, only the d_{xy} band is occupied. In this regime, transport is carried out with only one type of carrier and the spin splitting is expected to be rather small, since the Rashba parameter is only a few meV^{68,69}). By increasing the carrier density, the d_{xz} and d_{yz} bands become populated and their Rashba coefficient is calculated to have a sign opposite to one of the d_{xy} band^{62,70}). At an energy level close to the crossing of both light and heavy bands the Rashba parameter increases about one order of magnitude as a result of the strong mixing between both orbital characters. Naturally, this level of tunability of the Rashba coefficient unlocks the possibility to tune both the amplitude and the sign of the spin-to-charge conversion, by shifting between one-band and multi-band occupation.

Such experiments were demonstrated by Lesne et al. in NiFe/LAO/STO heterostructures⁷¹). The NiFe layer is used to pump a pure spin current towards the 2DEG formed at the LAO/STO interface, where it is converted into a 2D charge current. A voltage peak was measured, which appears at the very same magnetic field corresponding to magnetization precession in a steady state in FMR experiments (see Figure 2a). The conversion efficiency was tuned through electrostatic doping by using back-gate voltage, as displayed in Figure 2b. For negative gate voltages the 2DEG is depopulated to a carrier density of about $1 \times 10^{13} \text{ cm}^{-2}$. With the Fermi level at a lower position, only the light d_{xy} band is occupied, so that the charge current measured is low. As expected, by slightly changing the amplitude of the gate voltage (i.e. from -200V to -50 V) the current produced is almost unaltered, as no new bands were populated. For 0 V, the detected signal drops to zero, revealing that heavy $d_{xz/yz}$ bands start to be occupied and their Rashba coefficient starts to counteract the one from lighter bands. Reaching the crossing point, at about $3 \times 10^{13} \text{ cm}^{-2}$, the increasing Rashba parameter is accompanied by a peak in the charge current detected, corresponding to a $\lambda_{\text{REE}} = 6.4 \text{ nm}$. Note that this value is one order of magnitude higher than the one observed in Ag/Bi bilayer³³) and also higher than $\lambda_{\text{REE}} = 2.1 \text{ nm}$ found at the surface of the topological insulator $\alpha\text{-Sn}$ ⁴⁴). Additionally, a relaxation time of $\tau \sim 1.4 \text{ ps}$ can be derived for the given λ_{REE} and a Rashba parameter of $\alpha_{\text{R}} \sim 0.03 \text{ eV}\cdot\text{\AA}$ (deduced from theory⁷²) and magnetotransport measurements^{57,58}). At higher positive gate voltages, the signal decreases again, presumably due to the highly non-trivial interaction between other bands that become populated for higher carrier densities.

A priori, the results stated above for the LAO/STO interface are rather surprising,

considering that its Rashba parameter of $0.03 \text{ eV}\cdot\text{\AA}$ is one order of magnitude smaller than the $0.56 \text{ eV}\cdot\text{\AA}$ found for Bi (111) surface³³). However, since $\lambda_{\text{IREE}} \sim \alpha_{\text{R}}\tau$, one can understand the importance of having a protected high mobility 2DEG mediating the spin-to-charge conversion, thus providing higher momentum relaxation times than the ones found in conventional metal/metal interfaces.

Although the work by Lesne et al. was done at low temperatures, several other groups have investigated spin-to-charge conversion up to room temperature. At 300K, the dielectric constant of STO becomes as low as 300, compared to 20000 below 4 K, hampering the generation of large electric fields at the interface. Also, the mobility of charge carriers in the LAO/STO 2DEG is known to be $1000\text{-}5000 \text{ cm}^2/\text{V}\cdot\text{s}$ at low temperature, but two orders of magnitude lower at higher temperatures, driving the relaxation time to lower values. Chauleau et al. found that λ_{IREE} drops to 1 nm at 75 K and about 0.15 nm at room temperature⁷³). Contradictorily, other groups have found an increase of the detected IREE voltage with increasing temperature⁷⁴). In view of the decrease of the momentum relaxation time with temperature, these results seem hard to reconcile with a simple inverse Rashba-Edelstein picture. Lastly, Zhang et al. performed similar experiments on Ar+ irradiated STO and found a $\lambda_{\text{IREE}} = 0.23 \text{ nm}$ ⁷⁵). The low conversion efficiency might however be due to the increased roughness (and reduced mobility of the 2DEG).

Regarding the reciprocal effect, experimental results on the REE are still scarce. Wang et al.⁷⁶) have demonstrated through ST-FMR experiments that when driving a RF charge current through the LAO/STO 2DEG (see Figure 2c), a non-equilibrium spin density is propagated perpendicularly towards the ferromagnetic top layer. This leads to magnetization precession under the influence of the induced damping-like torque, revealed by the large symmetric contribution to the measured voltage signal (Figure 2d). The charge-to-spin conversion efficiency was estimated to be $q_{\text{REE}} = 0.63 \text{ nm}^{-1}$ at room temperature and was found to fall drastically when temperature decreases. This decrease was attributed to a lower conduction of spin-polarized electrons through defect states in the LAO barrier.

Using a Hall-bar like geometry, Jin et al. demonstrated charge-to-spin and spin-to-charge conversion within the same device⁷⁷). In these experiments, a charge current injected between the source and the drain induces a perpendicular spin current (through the REE). The spin current propagates in the 2DEG channel, is reconverted to a charge current (through IREE) and gets nonlocally detected at the adjacent contacts of the Hall-bar (see Figure 2e). Since the propagating spin current has a polarization perpendicular to the

plane, applying an in-plane magnetic field induces Larmor precession of the spins, so that for large enough fields the spins will become parallel to the plane. This effect can be seen in Figure 2f, where Hanle experiments showed a decrease of the detected voltage with increasing magnetic field.

Additionally, anisotropic magnetoresistance measurements suggest that the REE might also be responsible for the appearance of a unidirectional component in transport⁷⁸⁾. Depending on the magnetization direction of the magnetic overlayer, the produced spin current might be either absorbed (through spin-transfer torque) or reflected, allowing two different resistive states. This effect, labeled unidirectional spin Hall magnetoresistance, have been demonstrated in ferromagnet/metal bilayers⁷⁹⁾ and other topological systems^{80,81)}, but is yet to be realized for oxide-based heterostructures. Finally, let us mention that IREE has also been reported at the interface of other oxides such as Bi_2O_3 ⁸²⁾, which provides another approach for spin-charge interconversion with oxide materials.

5. Conclusion

The broad variety of properties displayed by transition metal oxides, especially perovskites, and their excellent structural compatibility are key features to their integration into countless types of multifunctional devices. Although the energies driving their physical response are usually related to crystal field (with corresponding level splitting due to oxygen rotations, Jahn-Teller distortions and polar shifts) and to on-site Coulomb repulsion (strong electronic correlations), spin-orbit coupling should not be neglected and may in fact produce phenomena of giant amplitude, as illustrated by the record inverse and direct Rashba-Edelstein effect observed in $\text{LaAlO}_3/\text{SrTiO}_3$. Importantly, in such SrTiO_3 -based systems, electrons in the 2DEG are protected from leakage towards neighboring metals by a potential barrier (e.g. a thin LaAlO_3 film), which provides an optimization route to achieve long scattering times at room temperature⁸³⁾. However, attempts to quantify the influence of spin-orbit coupling through transport measurements in oxides have been scarce so far. Yet, with several metallic compounds with 4d and 5d elements, perovskites are promising materials for efficient direct and inverse spin Hall effects, and systematic investigations should be undertaken. In addition, the strongly ionic nature of most oxides implies that the electric fields generated at interfaces between dissimilar compounds can be larger than with other materials families. If one of the materials is a ferroelectric, this can be an efficient way to achieve strong Rashba coefficients, which may be electrically tunable in a non-volatile way. In parallel, novel materials beyond perovskites may also be

interesting candidates, as illustrated by the giant Rashba splitting recently discovered in delafossites⁸⁴).

Acknowledgements

The authors thank A. Fert for useful discussions. This work was supported by the ERC Consolidator Grant #615759 "MINT", the French Research Agency (ANR) as part of the "Investissement d'Avenir" program (LABEX NanoSaclay, ref. ANR-10-LABX-0035) through project "AXION" and the ANR project "OISO".

References

- 1) Chappert, C., A. Fert & F. Nguyen Van Dau. *Nat. Mater.* **6**, 813–817 (2007).
- 2) Slonczewski, J. C. J. *Magn. Magn. Mater.* **159**, L1–L7 (1996).
- 3) Myers, E. B., D. C. Ralph, J. A. Katine, R. N. Louie & R. A. Buhrman. *Science* (80-.). **285**, 867–870 (1999).
- 4) Hill, N. A. *J. Phys. Chem. B* **104**, 6694–6709 (2000).
- 5) Ramesh, R. & N. A. Spaldin. *Nat. Mater.* **6**, 21–29 (2007).
- 6) Cheong, S.-W. & M. Mostovoy. *Nat. Mater.* **6**, 13–20 (2007).
- 7) Fusil, S., V. Garcia, A. Barthélémy & M. Bibes. *Annu. Rev. Mater. Res.* **44**, 91–116 (2014).
- 8) Maruyama, T., Y. Shiota, T. Nozaki, K. Ohta, N. Toda, M. Mizuguchi, A. A. Tulapurkar, T. Shinjo, M. Shiraishi, S. Mizukami, Y. Ando & Y. Suzuki. *Nat. Nanotechnol.* **4**, 158–161 (2009).
- 9) Zhao, T., A. Scholl, F. Zavaliche, K. Lee, M. Barry, A. Doran, M. P. Cruz, Y. H. Chu, C. Ederer, N. a Spaldin, R. R. Das, D. M. Kim, S. H. Baek, C. B. Eom & R. Ramesh. *Nat. Mater.* **5**, 823–829 (2006).
- 10) Chu, Y., L. W. Martin, M. B. Holcomb, M. Gajek, S. Han, Q. He, N. Balke, C. Yang, D. Lee, W. Hu, Q. Zhan, P. Yang, A. Fraile-Rodríguez, A. Scholl, S. X. Wang & R. Ramesh. *Nat. Mater.* **7**, 478–482 (2008).
- 11) Allibe, J., I. C. Infante, S. Fusil, K. Bouzehouane, E. Jacquet, C. Deranlot, M. Bibes & A. Barthélémy. *Appl. Phys. Lett.* **95**, 182503 (2009).
- 12) Allibe, J., S. Fusil, K. Bouzehouane, C. Daumont, D. Sando, E. Jacquet, C. Deranlot & M. Bibes. *Nano Lett.* **12**, 1141–1145 (2012).
- 13) Heron, J. T., J. L. Bosse, Q. He, Y. Gao, M. Trassin, L. Ye, J. D. Clarkson, C. Wang, J. Liu, S. Salahuddin, D. C. Ralph, D. G. Schlom, J. Íñiguez, B. D. Huey, R. Ramesh,

- J. Iñiguez, B. D. Huey & R. Ramesh. *Nature* **516**, 370–373 (2014).
- 14) Cherifi, R. O., V. Ivanovskaya, L. C. Phillips, A. Zobelli, I. C. Infante, E. Jacquet, V. Garcia, S. Fusil, P. R. Briddon, N. Guiblin, A. Mougin, A. A. Ünal, F. Kronast, S. Valencia, B. Dkhil, A. Barthélémy & M. Bibes. *Nat. Mater.* **13**, 345–351 (2014).
 - 15) Manipatruni, S., D. E. Nikonov & I. A. Young. *Arxiv Prepr.* **23**, 1512.05428 (2015).
 - 16) Manipatruni, S., D. E. Nikonov, C. Lin, P. Bhagwati, Y. L. Huang, A. R. Damodaran, Z. Chen, R. Ramesh & I. A. Young. *ArXiv Prepr.* 1801.08280 (2018).
 - 17) Sando, D., A. Barthélémy & M. Bibes. *J. Phys. Condens. Matter* **26**, 473201 (2014).
 - 18) D'Yakonov, M. I. & V. I. Perel. *JETP Lett.* **13**, 467 (1971).
 - 19) Kato, Y. K., R. C. Myers, A. C. Gossard & D. D. Awschalom. *Science* **306**, 1910–1913 (2004).
 - 20) Saitoh, E., M. Ueda, H. Miyajima & G. Tatara. *Appl. Phys. Lett.* **88**, 182509 (2006).
 - 21) Valenzuela, S. O. & M. Tinkham. *Nature* **442**, 176–179 (2006).
 - 22) Liu, L., T. Moriyama, D. C. Ralph & R. A. Buhrman. *Phys. Rev. Lett.* **106**, 36601 (2011).
 - 23) Liu, L., C. Pai, Y. Li, H. W. Tseng, D. C. Ralph & R. A. Buhrman. *Science* **336**, 555–558 (2012).
 - 24) Khvalkovskiy, A. V., V. Cros, D. Apalkov, V. Nikitin, M. Krounbi, K. a. Zvezdin, A. Anane, J. Grollier & A. Fert. *Phys. Rev. B* **87**, 20402 (2013).
 - 25) Demidov, V. E., S. Urazhdin, H. Ulrichs, V. Tiberkevich, A. Slavin, D. Baither, G. Schmitz & S. O. Demokritov. *Nat. Mater.* **11**, 1028–1031 (2012).
 - 26) Gladii, O., M. Collet, K. Garcia-Hernandez, C. Cheng, S. Xavier, P. Bortolotti, V. Cros, Y. Henry, J. V. Kim, A. Anane & M. Bailleul. *Appl. Phys. Lett.* **108**, 202407 (2016).
 - 27) Evelt, M., V. E. Demidov, V. Bessonov, S. O. Demokritov, J. L. Prieto, M. Muñoz, J. Ben Youssef, V. V. Naletov, G. De Loubens, O. Klein, M. Collet, K. Garcia-Hernandez, P. Bortolotti, V. Cros & A. Anane. *Appl. Phys. Lett.* **108**, 172406 (2016).
 - 28) Manchon, A., H. C. Koo, J. Nitta, S. M. Frolov & R. A. Duine. *Nat. Mater.* **14**, 871–882 (2015).
 - 29) Kondou, K., R. Yoshimi, A. Tsukazaki, Y. Fukuma, J. Matsuno, K. S. Takahashi, M. Kawasaki, Y. Tokura & Y. Otani. *Nat. Phys.* **12**, 1027–1031 (2016).
 - 30) Kim, J., Y. T. Chen, S. Karube, S. Takahashi, K. Kondou, G. Tatara & Y. Otani. *Phys. Rev. B* **96**, 140409 (2017).

- 31) Zhang, S. & A. Fert. *Phys. Rev. B* **94**, 184423 (2016).
- 32) Zhang, X., L. B. Abdalla, Q. Liu & A. Zunger. *New J. Phys.* **18**, 125014 (2016).
- 33) Sánchez, J. C. R., L. Vila, G. Desfonds, S. Gambarelli, J. P. Attané, J. M. De Teresa, C. Magén & A. Fert. *Nat. Commun.* **4**, 2944 (2013).
- 34) Zhang, H. J., S. Yamamoto, B. Gu, H. Li, M. Maekawa, Y. Fukaya & A. Kawasuso. *Phys. Rev. Lett.* **114**, 166602 (2015).
- 35) Zhang, W., M. B. Jungfleisch, W. Jiang, J. E. Pearson, A. Hoffmann, W. Zhang, M. B. Jungfleisch, W. Jiang, J. E. Pearson & A. Hoffmann. *J. Appl. Phys.* **117**, 17C727 (2015).
- 36) Isasa, M., M. C. Martínez-Velarte, E. Villamor, C. Magén, L. Morellón, J. M. De Teresa, M. R. Ibarra, G. Vignale, E. V. Chulkov, E. E. Krasovskii, L. E. Hueso & F. Casanova. *Phys. Rev. B* **93**, 23–27 (2016).
- 37) Mendes, J. B. S., O. Alves Santos, L. M. Meireles, R. G. Lacerda, L. H. Vilela-Leão, F. L. A. Machado, R. L. Rodríguez-Suárez, A. Azevedo & S. M. Rezende. *Phys. Rev. Lett.* **115**, 226601 (2015).
- 38) Dushenko, S., H. Ago, K. Kawahara, T. Tsuda, S. Kuwabata, T. Takenobu, T. Shinjo, Y. Ando & M. Shiraishi. *Phys. Rev. Lett.* **116**, 166102 (2016).
- 39) MacNeill, D., G. M. Stiehl, M. H. D. Guimaraes, R. A. Buhrman, J. Park & D. C. Ralph. *Nat. Phys.* **13**, 300–305 (2017).
- 40) Mellnik, A. R., J. S. Lee, A. Richardella, J. L. Grab, P. J. Mintun, M. H. Fischer, A. Vaezi, A. Manchon, E. A. Kim, N. Samarth & D. C. Ralph. *Nature* **511**, 449–451 (2014).
- 41) Li, C. H., O. M. J. van 't Erve, J. T. Robinson, Y. Liu, L. Li & B. T. Jonker. *Nat. Nanotechnol.* **9**, 218–224 (2014).
- 42) Fan, Y., P. Upadhyaya, X. Kou, M. Lang, S. Takei, Z. Wang, J. Tang, L. He, L. Chang, M. Montazeri, G. Yu, W. Jiang, T. Nie, R. N. Schwartz, Y. Tserkovnyak & K. L. Wang. *Nat. Mater.* **13**, 699–704 (2014).
- 43) Shiomi, Y., K. Nomura, Y. Kajiwara, K. Eto, M. Novak, K. Segawa, Y. Ando & E. Saitoh. *Phys. Rev. Lett.* **113**, 196601 (2014).
- 44) Rojas-Sánchez, J. C., S. Oyarzún, Y. Fu, A. Marty, C. Vergnaud, S. Gambarelli, L. Vila, M. Jamet, Y. Ohtsubo, A. Taleb-Ibrahimi, P. Le Fèvre, F. Bertran, N. Reyren, J. M. George & A. Fert. *Phys. Rev. Lett.* **116**, 96602 (2016).
- 45) Song, Q., J. Mi, D. Zhao, T. Su, W. Yuan, W. Xing, Y. Chen, C. Luo, et al. *Nat. Commun.* **7**, 13485 (2016).

- 46) Mihai Miron, I., G. Gaudin, S. Auffret, B. Rodmacq, A. Schuhl, S. Pizzini, J. Vogel & P. Gambardella. *Nat. Mater.* **9**, 230–234 (2010).
- 47) Qiu, Z., Y. Kajiwara, K. Ando, Y. Fujikawa, K. Uchida, T. Tashiro, K. Harii, T. Yoshino & E. Saitoh. *Appl. Phys. Lett.* **100**, 22402 (2012).
- 48) Qiu, Z., T. An, K. Uchida, D. Hou, Y. Shiomi, Y. Fujikawa & E. Saitoh. *Appl. Phys. Lett.* **103**, 182404 (2013).
- 49) Fujiwara, K., Y. Fukuma, J. Matsuno, H. Idzuchi, Y. Niimi, Y. Otani & H. Takagi. *Nat. Commun.* **4**, 2893 (2013).
- 50) Bibes, M., J. E. Villegas & A. Barthélémy. *Adv. Phys.* **60**, 5–84 (2011).
- 51) Qin, Q., S. He, W. Song, P. Yang, Q. Wu, Y. P. Feng & J. Chen. *Appl. Phys. Lett.* **110**, 112401 (2017).
- 52) Ohtomo, A. & H. Y. Hwang. *Nature* **427**, 423–426 (2004).
- 53) Reyren, N., S. Thiel, A. D. Caviglia, L. Fitting Kourkoutis, G. Hammerl, C. Richter, C. W. Schneider, T. Kopp, A.-S. Rüetschi, D. Jaccard, M. Gabay, D. A. Muller, J.-M. Triscone & J. Mannhart. *Science* **317**, 1196–1199 (2007).
- 54) Bert, J. A., B. Kalisky, C. Bell, M. Kim, Y. Hikita, H. Y. Hwang & K. A. Moler. *Nat. Phys.* **7**, 767–771 (2011).
- 55) Salluzzo, M., S. Gariglio, D. Stornaiuolo, V. Sessi, S. Rusponi, C. Piamonteze, G. M. De Luca, M. Minola, D. Marré, A. Gadaleta, H. Brune, F. Nolting, N. B. Brookes & G. Ghiringhelli. *Phys. Rev. Lett.* **111**, 87204 (2013).
- 56) Lee, J.-S., Y. W. Xie, H. K. Sato, C. Bell, Y. Hikita, H. Y. Hwang & C.-C. Kao. *Nat. Mater.* **12**, 703–706 (2013).
- 57) Caviglia, A. D., M. Gabay, S. Gariglio, N. Reyren, C. Cancellieri & J. M. Triscone. *Phys. Rev. Lett.* **104**, 126803 (2010).
- 58) Hurand, S., A. Jouan, C. Feuillet-Palma, G. Singh, J. Biscaras, E. Lesne, N. Reyren, A. Barthélémy, M. Bibes, J. E. Villegas, C. Ulysse, X. Lafosse, M. Pannetier-Lecoœur, S. Caprara, M. Grilli, J. Lesueur & N. Bergeal. *Sci. Rep.* **5**, 12751 (2015).
- 59) Fête, A., S. Gariglio, A. D. Caviglia, J.-M. Triscone & M. Gabay. *Phys. Rev. B* **86**, 201105 (2012).
- 60) Ben Shalom, M., M. Sachs, D. Rakhmilevitch, A. Palevski & Y. Dagan. *Phys. Rev. Lett.* **104**, 126802 (2010).
- 61) Gopinadhan, K., A. Annadi, Y. Kim, A. Srivastava, B. Kumar, J. Chen, J. M. D. Coey & T. Venkatesan. *Adv. Mater.* **3**, 1500114 (2015).

- 62) Shanavas, K. V. & S. Satpathy. *Phys. Rev. Lett.* **112**, 86802 (2014).
- 63) Zhong, Z., A. Tóth & K. Held. *Phys. Rev. B* **87**, 161102 (2013).
- 64) Bucheli, D., M. Grilli, F. Peronaci, G. Seibold & S. Caprara. *Phys. Rev. B* **89**, 195448 (2014).
- 65) Liang, H., L. Cheng, L. Wei, Z. Luo, G. Yu, C. Zeng & Z. Zhang. *Phys. Rev. B* **92**, 75309 (2015).
- 66) Salluzzo, M., J. C. Cezar, N. B. Brookes, V. Bisogni, G. M. De Luca, C. Richter, S. Thiel, J. Mannhart, M. Huijben, A. Brinkman, G. Rijnders & G. Ghiringhelli. *Phys. Rev. Lett.* **102**, 166804 (2009).
- 67) Lesne, E., N. Reyren, D. Doennig, R. Mattana, H. Jaffrès, V. Cros, F. Petroff, F. Choueikani, P. Ohresser, R. Pentcheva, A. Barthélémy & M. Bibes. *Nat. Commun.* **5**, 4291 (2014).
- 68) King, P. D. C., S. McKeown Walker, a Tamai, a de la Torre, T. Eknapakul, P. Buaphet, S.-K. Mo, W. Meevasana, M. S. Bahramy & F. Baumberger. *Nat. Commun.* **5**, 3414 (2014).
- 69) Walker, S. M. K., F. Y. Bruno, Z. Wang, A. De La Torre, S. Riccò, A. Tamai, T. K. Kim, M. Hoesch, M. Shi, M. S. Bahramy, P. D. C. King & F. Baumberger. *Adv. Mater.* **27**, 3894–3899 (2015).
- 70) Joshua, A., S. Pecker, J. Ruhman, E. Altman & S. Ilani. *Nat. Commun.* **3**, 1129 (2012).
- 71) Lesne, E., Y. Fu, S. Oyarzun, J. C. Rojas-Sánchez, D. C. Vaz, H. Naganuma, G. Sicoli, J.-P. Attané, M. Jamet, E. Jacquet, J.-M. George, A. Barthélémy, H. Jaffrès, A. Fert, M. Bibes & L. Vila. *Nat. Mater.* **15**, 1261–1266 (2016).
- 72) Shanavas, K. V., Z. S. Popović & S. Satpathy. *Phys. Rev. B* **90**, 165108 (2014).
- 73) Chauleau, J.-Y., M. Boselli, S. Gariglio, R. Weil, G. de Loubens, J.-M. Triscone & M. Viret. *Europhys. Lett.* **116**, 17006 (2016).
- 74) Song, Q., H. Zhang, T. Su, W. Yuan, Y. Chen, W. Xing, J. Shi, J. Sun & W. Han. *Sci. Adv.* **3**, e1602312 (2017).
- 75) Zhang, W., Q. Wang, B. Peng, H. Zeng, W. T. Soh, C. K. Ong & W. Zhang. *Appl. Phys. Lett.* **109**, 262402 (2016).
- 76) Wang, Y., R. Ramaswamy, M. Motapothula, K. Narayanapillai, D. Zhu, J. Yu, T. Venkatesan & H. Yang. *Nano Lett.* **17**, 7659–7664 (2017).
- 77) Jin, M. J., S. Y. Moon, J. Park, V. Modepalli, J. Jo, S. I. Kim, H. C. Koo, B. C. Min, H. W. Lee, S. H. Baek & J. W. Yoo. *Nano Lett.* **17**, 36–43 (2017).

- 78) Narayanapillai, K., K. Gopinadhan, X. Qiu, A. Annadi, Ariando, T. Venkatesan & H. Yang. *Appl. Phys. Lett.* **105**, 162405 (2014).
- 79) Avci, C. O., K. Garello, A. Ghosh, M. Gabureac, S. F. Alvarado & P. Gambardella. *Nat. Phys.* **11**, 570–575 (2015).
- 80) Yasuda, K., A. Tsukazaki, R. Yoshimi, K. S. Takahashi, M. Kawasaki & Y. Tokura. *Phys. Rev. Lett.* **117**, 127202 (2016).
- 81) Lv, Y., J. Kally, D. Zhang, J. S. Lee, M. Jamali, N. Samarth & J.-P. Wang. *Nat. Commun.* **9**, 111 (2018).
- 82) Karube, S., K. Kondou & Y. C. Otani. *Appl. Phys. Express* **9**, 33001 (2016).
- 83) Şahin, C., G. Vignale & M. E. Flatté. *Phys. Rev. B - Condens. Matter Mater. Phys.* **89**, 155402 (2014).
- 84) Sunko, V., H. Rosner, P. Kushwaha, S. Khim, F. Mazzola, L. Bawden, O. J. Clark, J. M. Riley, D. Kasinathan, M. W. Haverkort, T. K. Kim, M. Hoesch, J. Fujii, I. Vobornik, A. P. Mackenzie & P. D. C. King. *Nature* **549**, 492–496 (2017).
- 85) Soumyanarayanan, A., N. Reyren, A. Fert & C. Panagopoulos. *Nature* **539**, 509–517 (2016).
- 86) Lesne, E, Ph.D. Thesis. Université Pierre et Marie Curie, France (2015).
- 87) Y. Tokura, Y. Taguchi, Y. Okada, T. Fujishima, T. Arima, K. Kumagai & Y. Iye. *Phys. Rev. Lett.* **70**, 2126 (1993).
- 88) Son, J., P. Moetakef, B. Jalan, O. Bierwagen, N. J. Wright, R. Engel-Herbert & S. Stemmer. *Nat. Mater.* **9**, 482–484 (2010).
- 89) Onoda, M., H. Ohta & H. Nagasawa. *Solid State Commun.* **79**, 281–285 (1991).
- 90) Zhang, K. H. L., Y. Du, P. V Sushko, M. E. Bowden, V. Shutthanandan, S. Sallis, L. F. J. Piper & S. A. Chambers. *Phys. Rev. B* **91**, 155129 (2015).
- 91) Urushibara, A., Y. Moritomo, T. Arima, A. Asamitsu, G. Kido & Y. Tokura. *Phys. Rev. B* **51**, 14103–14109 (1995).
- 92) Ishiwata, S., M. Tokunaga, Y. Kaneko, D. Okuyama, Y. Tokunaga, S. Wakimoto, K. Kakurai, T. Arima, Y. Taguchi & Y. Tokura. *Phys. Rev. B* **84**, 54427 (2011).
- 93) Oka, D., Y. Hirose, S. Nakao, T. Fukumura & T. Hasegawa. *Phys. Rev. B* **92**, 205102 (2015).
- 94) Nagai, I., N. Shirakawa, S. I. Ikeda, R. Iwasaki, H. Nishimura & M. Kosaka. *Appl. Phys. Lett.* **87**, 85–88 (2005).
- 95) Rao, R. A., Q. Gan, C. B. Eom, R. J. Cava, Y. Suzuki, J. J. Krajewski, S. C. Gausepohl & M. Lee. *Appl. Phys. Lett.* **70**, 3035–3037 (1997).

- 96) Yamaura, K., Q. Huang, D. P. Young, M. Arai & E. Takayama-Muromachi. *Phys. B* **329–333**, 820–821 (2002).
- 97) Wemple, S. H. *Phys. Rev.* **137**, A1575–A1582 (1965).
- 98) Berak, J. M. & M. J. Sienko. *J. Solid. State Chem.* **2**, 109–133 (1970).
- 99) Tanaka, T., T. Akahane, E. Bannai, S. Kawai, N. Tsuda & Y. Ishizawa. *J. Phys. C Solid State Phys.* **9**, 1235 (1976).
- 100) Shi, Y., Y. Guo, Y. Shirako, W. Yi, X. Wang, A. A. Belik, Y. Matsushita, H. L. Feng, Y. Tsujimoto, M. Arai, N. Wang, M. Akaogi & K. Yamaura. *J. Am. Chem. Soc.* **135**, 16507–16516 (2013).
- 101) Wu, F., J. Zhou, L. Y. Zhang, Y. B. Chen, S. Zhang, Z. Gu, S. Yao & Y. Chen. *J. Phys. Condens. Matter* **25**, 125604 (2013).

Figure Caption

Figure 1 - (a) Representative sketch of the Spin Hall effect. When an electrical current passes through a non-magnetic metal with SOC, spin accumulations appear on the two surfaces of the sample perpendicular to the charge current applied. In other words, a pure spin current perpendicular to the charge current is generated. Conversely, a pure spin current injected through a material with SOC will generate a transverse charge current; the Inverse Spin Hall Effect (ISHE). (b) The momentum-dependent spin split subbands plotted as brown and blue parabolic lines in the (k_x, k_y) -E plot. In a Rashba system, this spin splitting is caused by broken inversion symmetry and SO interaction that lift the spin degeneracy of the band structure⁸⁵. (c) Representation of the Rashba-Edelstein Effect (REE). A charge current (j_c) injected at the interface along -x induces a shift Δk_x of both Fermi contours, resulting in a spin accumulation polarized along the y axis due to the inequivalence of the two contours. (d) Representation of the Inverse Rashba-Edelstein Effect (IREE). When a spin current is injected perpendicularly to the 2DEG with the spin polarization along the y axis, the spin population is altered in the steady state causing a displacement in momentum space of the two inequivalent Fermi surfaces (red and blue lines) by $\pm \Delta k_x$. This results in a net charge current generated perpendicularly to the spin current and to its spin polarization⁸⁶.

Figure 2 – (a) Schematic of the FMR-spin pumping measurement configuration. Two contacts are made to probe the voltage generated through the IREE after the injection of a pure spin current into the 2DEG through spin pumping. A third contact is used as back-gate voltage, allowing an electrostatic tuning of the properties of the 2DEG and ultimately a

modulation of the generated charge current. **(b)** Gate dependence of the spin-to-charge conversion efficiency λ_{IRRE} . A sketch of the band structure is presented in the inset. The colored shaded area represents the assumed swept region using gate voltage. At about +125 V, the Fermi level is at the avoided crossing point, where the Rashba coefficient α_{R} is expected to be the largest. **(c)** Schematic of a charge-to-spin conversion configuration. An applied RF charge current passing through the 2DEG generates a perpendicular spin accumulation through the REE. Considering that a static d.c. magnetic field is applied in a different direction compared to the incoming spin polarization, precession of the FM magnetization is triggered through torque transfer. If the spin current generated is large enough, magnetization switching in the FM might occur. **(d)** ST-FMR detected voltage at FMR resonance, including both symmetric and antisymmetric Lorentzian components. **(e)** Schematic of the Hall-bar like nonlocal spin detection configuration. A charge current injected between source and drain is converted into a spin current and then reconverted back to a charge current, to be finally detected in the adjacent contacts. **(f)** The nonlocal voltage detected as a function of the applied in-plane magnetic field generates a Hanle curve.

Table 1 - Examples of metallic perovskite oxides based on different 3d, 4d and 5d transition metals. All mentioned 4d and 5d, as well as Ti, V and Ni compounds do not show magnetic ordering. Some of the mentioned Cr, Mn and Co compounds as well as SrFeO_3 are magnetic below some critical temperature but maintain a metallic behavior in the paramagnetic state.

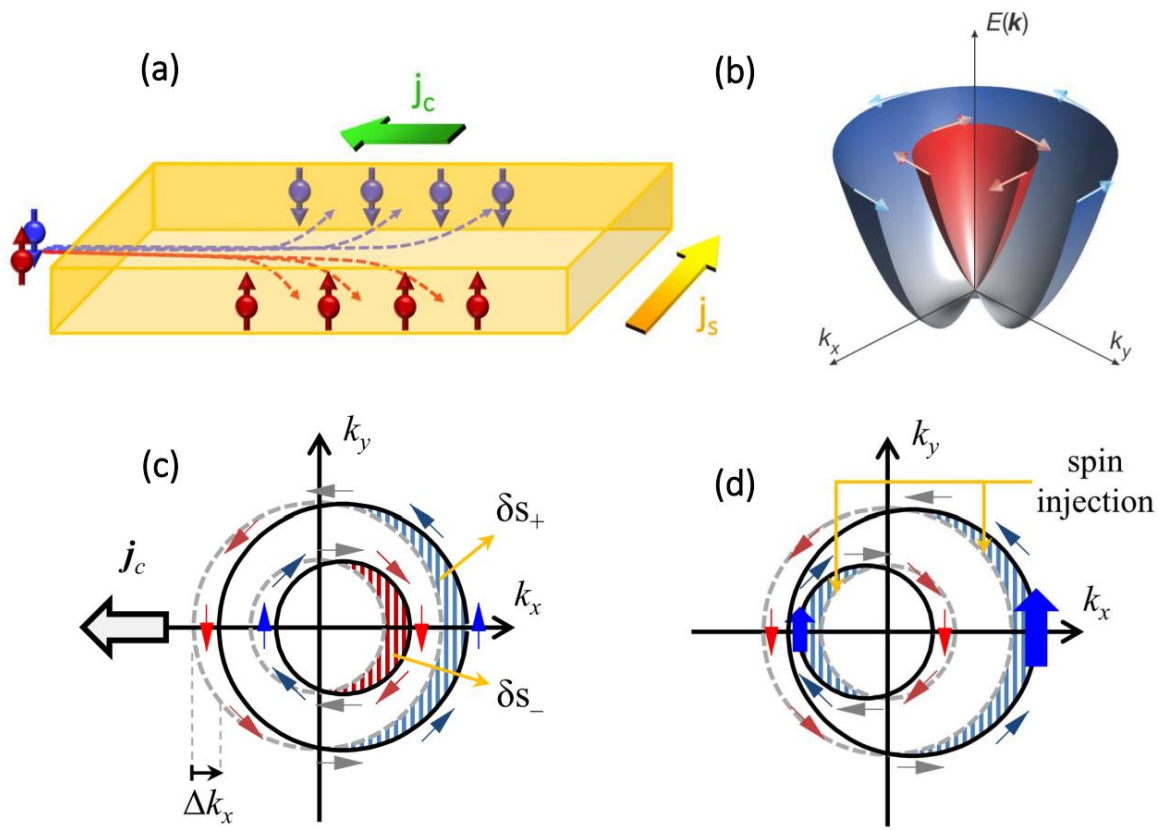


Figure 1

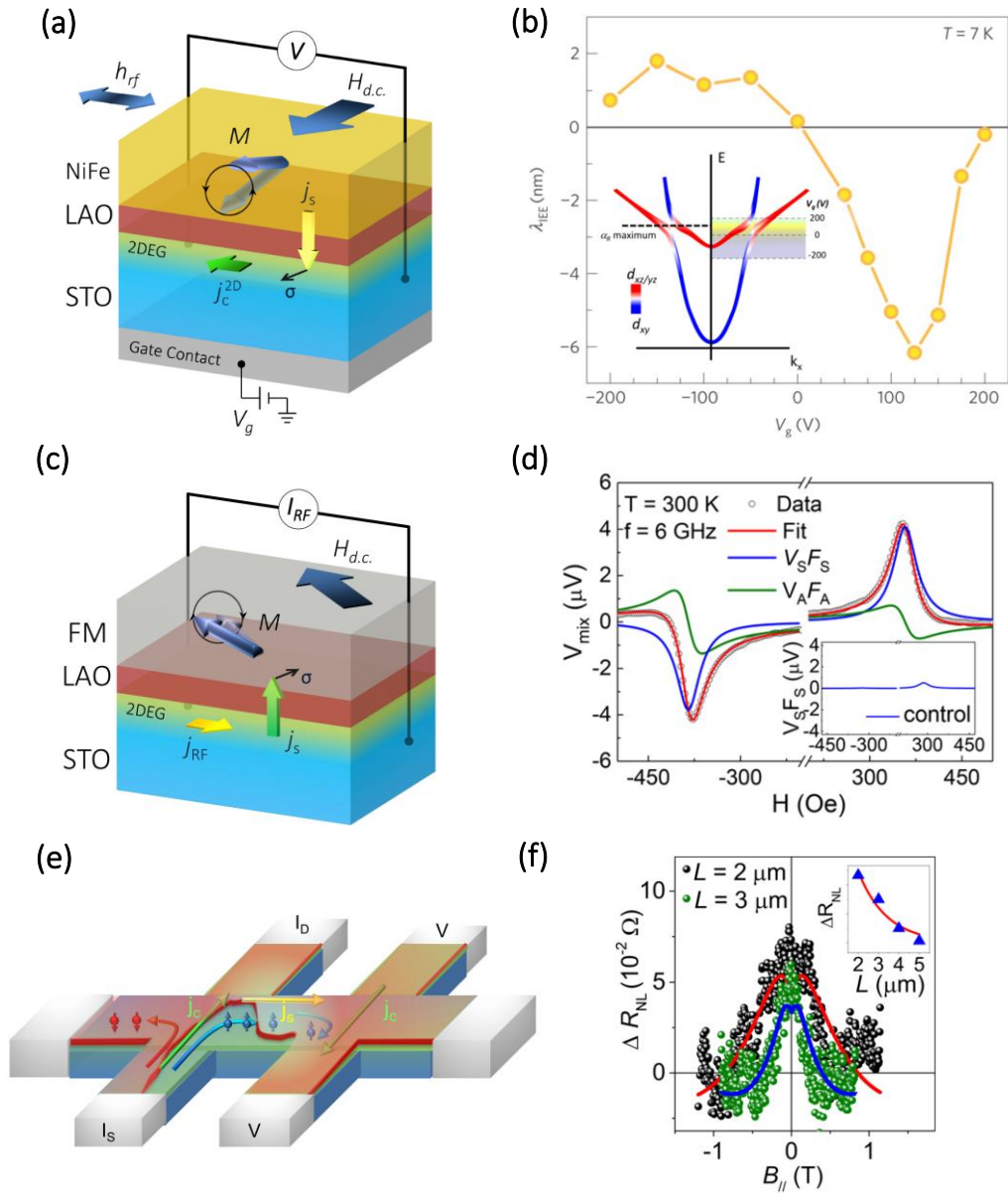


Figure 2

3d	Sc	Ti	V	Cr	Mn	Fe	Co	Ni	Cu	Zn
	--	La _{1-x} Sr _x TiO ₃ 10 ⁻³ ≤ x ≤ 0.95 87,88)	SrVO ₃ 89)	La _{1-x} Sr _x CrO ₃ 0.65 ≤ x 90)	La _{1-x} Sr _x MnO ₃ 0.17 ≤ x ≤ 0.6 91)	SrFeO ₃ 92)	La _{1-x} Sr _x CoO ₃	LaNiO ₃	--	--
4d	Y	Zr	Nb	Mo	Tc	Ru	Rh	Pd	Ag	Cd
	--	--	SrNbO ₃ 93)	SrMoO ₃ 94)	--	CaRuO ₃ 95)	SrRhO ₃ 96)	--	--	--
5d	--	Hf	Ta	W	Re	Os	Ir	Pt	Au	Hg
		--	KTaO _{3-d} 97)	WO _{3-d} 98)	ReO ₃ 99)	SrOsO ₃ 100)	SrIrO ₃ 101)	--	--	--

Table 1